Analytical performance and validations of the Galileo five-frequency precise point positioning models

Ke Su [a,b], Shuanggen Jin [a,c,d,*]

[a] Shanghai Astronomical Observatory, Chinese Academy of Sciences, Shanghai 200030, China
[b] University of Chinese Academy of Sciences, Beijing 100049, China
[c] School of Remote Sensing and Geomatics Engineering, Nanjing University of Information Science and Technology, Nanjing 210044, China
[d] Jiangsu Engineering Center for Collaborative Navigation/Positioning and Smart Applications, Nanjing 210044, China

ARTICLE INFO

ABSTRACT

Galileo navigation satellite system provides global services with five-frequency signals. The contribution of this study is to develop four Galileo five-frequency precise point positioning (PPP) models with the ionospheric-free (IF) and uncombined observables, namely FF1, FF2, FF3 and FF4 models, respectively. Galileo dual- and triple-frequency IF models, known as DF and TF models, are also investigated for comparisons. The Galileo dual- and multi-frequency PPP models are comprehensively evaluated with thirty consecutive days period observations collected from 26 multi-GNSS experiment (MGEX) network stations, together with a dynamic experiment dataset, in terms of the static and kinematic performance. The by-product estimated parameters in five-frequency PPP models including the receiver clock, tropospheric delay, receiver inter-frequency biases (IFBs) and differential code bias (DCB) are also analyzed. The experimental results show that the FF1, FF2, and FF3 models perform basic consistent and the FF4 model exhibits inconsistency due to the external ionospheric constraint. The Galileo kinematic PPP performance is significantly improved with the multi-frequency observations under the limited observed satellites circumstance. The significance and potency of the Galileo five-frequency PPP is demonstrated for future Galileo applications.

1. Introduction

Over the last few decades, the Global Navigation Satellite Systems (GNSSs) have made great progress with the construction of the Global Positioning System (GPS), BeiDou Navigation Satellite System (BDS), GNSS of Russia (GLONASS) and Galileo, as well as the Quasi-Zenith Satellite System (QZSS) and Indian Regional Navigation Satellite System (IRNSS), which have been operational with the transmission of multi-frequency signals [1–4]. Particularly as the European GNSS, Galileo system run by the European Space Agency (ESA) is able to provide positioning, navigation and timing (PNT) services to European citizens and worldwide [5–7]. The fully developed Galileo is capable of offering globally high-performance and reliable services including Open Service (OS), Public Regulated Service (PRS), Commercial Service (CS) and Search and Rescue Service (SAR) [8]. Galileo was designed independently to provide five-frequency signals centered at E1 (1575.42 MHz), E5a (1176.45 MHz), E5b (1207.14 MHz), E5 (1191.795 MHz) and E6

(1278.75 MHz), respectively, for civilian and commercial services [9–11].

With the Galileo five-frequency signals, more optimum advantages and choices can be obtained such as in the aspects of the low-noise level, ionosphere modeling and precise positioning, which has much potency in the Galileo applications [12,13]. Until now, many studies were investigated for the Galileo multi-frequency real-time kinematic (RTK) technology. For example, Tu *et al.* [14] proposed the four-frequency Galileo RTK model that uses one common reference satellite to achieve better positioning accuracy and ambiguity fix success rate. Wang *et al.* [15] performed the five-frequency Galileo RTK long-baseline ambiguity resolution with multipath mitigation to achieve high ambiguity success rate within a short time. For absolute stand-alone positioning, it starts with the pseudorange-based positioning. Tian *et al* [16] analyzed the Galileo single point positioning (SPP) performance with 4 in-orbit validation (IOV) and 14 full operational capability (FOC) satellites, indicating that Galileo exhibits the same accuracy as GPS. However, the multipath and noise of the pseudorange observations will degrade

positioning performance and mask the atomic clocks short-term stability. To seek for better positioning performance and higher stability, precise point positioning (PPP) can acquire high precision position with the pseudorange, carrier phase observations as well as the precise orbit and clock products [17].

As we all know, PPP technique is popular in the GNSS community and has the wide applications in geodynamic research for its high-accuracy positioning and flexible operation with a stand-alone receiver using the precise products provided by global institutions such as the international GNSS service (IGS) [18]. PPP needs to consider more about the observables modelling and more estimated parameters compared to the traditional double differenced relative positioning. Whereas the PPP major problem is the long convergence time, which will generally take scores of minutes before the positioning errors converge [19]. Diverse multi-frequency PPP studies have been performed and investigated. Pan *et al.* [20] comprehensively compared and evaluated the three GPS triple-frequency PPP models with the GPS Block IIF satellites. Guo *et al.* [21] assessed the BDS-2 triple-frequency PPP performance in both static and kinematic scenarios, indicating that three proposed PPP models agree well with each other. Su and Jin [22] presented three triple-frequency PPP models to perform carrier phase precise time and frequency transfer with the BDS-3 B1I, B3I and B2a signals. With regard to the Galileo PPP solutions, Afifi and El-Rabbany [23] introduced a new PPP model that combined single-frequency GPS/Galileo observations in between-satellite single-difference mode. Cai *et al.* [24] developed the dual-frequency PPP models to process the observations of all the four GNSS systems. Deo and El-Mowafy [25] proposed two new PPP models that can be used for Galileo triple-frequency data to accelerate convergence of carrier phase float ambiguities. Liu *et al.* [26] proposed the method of PPP ambiguity resolution (AR) using Galileo triple-frequency observations. Zhang *et al.* [27] focused on the Galileo quad-frequency PPP precise time and transfer performance with the E1, E5a, E5b and E5 observations. Li *et al.* [28] presented a new Galileo multi-frequency PPP with taking advantage of five-frequency observations for rapid AR.

In the current multi-GNSS era, the multi-frequency precise positioning technology will no doubt be popular [29,30]. However, the previous studies mainly focus on the performance of the multi-GNSS PPP models and the studies related to the Galileo five-frequency PPP models were not investigated. Various multi-frequency PPP models can be established with the different observables and ionospheric delays processing strategies using Galileo five-frequency observations. The focus of this study is to develop and analyze the five-frequency PPP performance with Galileo E1, E5a, E5b, E5 and E6 signals. To facilitate comparative analysis, the Galileo E1/E5a dual-frequency and E1/E5a/E5b triple-frequency ionospheric-free (IF) PPP models are considered as well. This paper is organized as following structure. First, we develop the Galileo dual-, triple and five-frequency PPP models and discuss their relationships and characteristics. Then, the static Galileo five-frequency PPP performance is evaluated and validated in terms of positioning accuracy and convergence time with the multi-GNSS Experiment (MGEX) network stations. The rest of the parameters including the receiver clock, zenith tropospheric delay (ZTD), receiver inter-frequency biases (IFBs) and E1/E5a differential code bias (DCB) are also analyzed, followed by the kinematic PPP performance verification using a dynamic experimental dataset. Finally, some conclusions are given.

2. Methodology

This section starts with the Galileo dual- and triple-frequency PPP models. Then we develop four Galileo five-frequency PPP mathematical models in detail, classified as IF based models and uncombined (UC) models. The characteristics of the PPP models are also discussed. The IF based PPP models with five-frequency Galileo measurements can be implemented by two means: on the one hand, measurements can be combined by some of the dual-frequency IF combinations. We define it as FF1 model. On the other hand, an optimal five-frequency IF combination can be obtained through the five-frequency observations, where the model is defined as FF2 model. The UC PPP model with five-frequency Galileo measurements can also be implemented by two means: one is that raw five-frequency measurements are employed without additional external information, which is defined as FF3 model. Another model called FF4 model is that the UC observations are processed plus with external ionospheric products.

2.1. DF: Model with a dual-frequency IF combined observable

The PPP model known as dual-frequency (DF) model utilizes the Galileo E1/E5a dual-frequency IF combined observables. With m available Galileo satellites observed, the DF model can be written as [31]:

$$\begin{cases} \begin{bmatrix} \boldsymbol{P}_{DF} \\ \boldsymbol{\Phi}_{DF} \end{bmatrix} = \begin{bmatrix} \boldsymbol{e}_2 \otimes \boldsymbol{B}, \boldsymbol{e}_2 \otimes \boldsymbol{e}_m, \boldsymbol{n}_2 \otimes (\boldsymbol{f}_{1,2}^T \cdot \Lambda_{1,2} \otimes \boldsymbol{I}_m) \end{bmatrix} \begin{bmatrix} \boldsymbol{x} \\ \bar{t}_r \\ \boldsymbol{a}' \end{bmatrix} + \begin{bmatrix} \boldsymbol{\varepsilon}_{P,DF} \\ \boldsymbol{\varepsilon}_{\Phi,DF} \end{bmatrix}, \\ \begin{bmatrix} \boldsymbol{f}_{1,2}^T \cdot (\boldsymbol{q}' \otimes c_{\boldsymbol{P}}) \cdot \boldsymbol{f}_{1,2} & \\ & \boldsymbol{f}_{1,2}^T \cdot (\boldsymbol{q}' \otimes c_{\Phi}) \cdot \boldsymbol{f}_{1,2} \end{bmatrix} \otimes \boldsymbol{Q}_m \end{cases} \tag{1}$$

where $\boldsymbol{P}$ and Φ denote the observed minus computed (OMC) pseudorange and carrier phase values vectors, respectively; $\boldsymbol{x}$ denotes the vector of three-dimension receiver position increments as well as the zenith wet delay (ZWD); $\boldsymbol{B}$ is the corresponding design matrix; $\bar{t}_r$ denotes the estimable receiver clock offset vector; $\boldsymbol{e}_m$ is the m-row vector with all 1's elements; $\boldsymbol{a}'^T = [\boldsymbol{a}_1^T, \boldsymbol{a}_2^T]$ denotes the vector of the ambiguities, in which $\boldsymbol{a}_i$ is the vector of the ith frequency carrier phase ambiguities; $\boldsymbol{f}_{m,n}^T = [\alpha_{(m,n)}, \beta_{(m,n)}] = [f_m^2, -f_n^2]/(f_m^2 - f_n^2), (m, n = 1, 2, 3, 4, 5)$ is the IF frequency factor vector, in which f denotes the corresponding frequency value; $\boldsymbol{n}_2 = [0, 1]^T$; $\Lambda_{m,n} = \text{diag}(\lambda_m, \lambda_n)$ denotes the diagonal matrix of corresponding wavelengths; $\boldsymbol{I}_m$ is the m-dimension identity matrix; $\boldsymbol{\varepsilon}_P$ and $\boldsymbol{\varepsilon}_\Phi$ denote the pseudorange and carrier phase observation noise vectors. Correspondingly, and c_Φ denote the pseudorange and carrier phase variance factors; $\boldsymbol{q}' = \text{diag}(q_1^2, q_2^2)$, in which q_i denotes the observation noise ratio; $\boldsymbol{Q}_m = \text{diag}(\sin^{-2}(E_1), \sin^{-2}(E_2), ..., \sin^{-2}(E_m))$ denotes the cofactor matrix, in which E denotes the satellite elevation angle; $\otimes$ denotes the Kronecker product operation.

2.2. TF: Model with a triple-frequency IF combined observable

The triple-frequency (TF) PPP model known as the TF model integrates the E1/E5a/E5b signals to one combined observable. The TF model with m observed Galileo satellites can be written as [32]:

$$\begin{cases} \begin{bmatrix} \boldsymbol{P}_{TF} \\ \boldsymbol{\Phi}_{TF} \end{bmatrix} = \begin{bmatrix} \boldsymbol{e}_2 \otimes \boldsymbol{B}, \boldsymbol{e}_2 \otimes \boldsymbol{e}_m, \boldsymbol{n}_2 \otimes (\boldsymbol{k}'^T \cdot \Lambda_{1,2,3} \otimes \boldsymbol{I}_m) \end{bmatrix} \begin{bmatrix} \boldsymbol{x} \\ \bar{t}_r \\ \boldsymbol{a}'' \end{bmatrix} + \begin{bmatrix} \boldsymbol{\varepsilon}_{P,TF} \\ \boldsymbol{\varepsilon}_{\Phi,TF} \end{bmatrix}, \\ \begin{bmatrix} \boldsymbol{k}'^T \cdot (\boldsymbol{q}'' \otimes c_{\boldsymbol{P}}) \cdot \boldsymbol{k}' & \\ & \boldsymbol{k}'^T \cdot (\boldsymbol{q}'' \otimes c_{\Phi}) \cdot \boldsymbol{k}' \end{bmatrix} \otimes \boldsymbol{Q}_m \end{cases}$$

$$\tag{2}$$

where $k^{'T} = [k_1', k_2', k_3']$, in which k_1', k_2' and k_3' denote the triple-frequency combined coefficients. $\Lambda_{1,2,3} = \text{diag}(\lambda_1, \lambda_2, \lambda_3)$; $a^{''T} = [a_1^T, a_2^T, a_3^T]$ denotes the vector of the ambiguities; $q'' = \text{diag}(q_1^2, q_2^2, q_3^2)$.

2.3. FF1: Model with four dual-frequency IF combined observables

Any two of Galileo E1, E5a, E5b, E5 and E6 observations can be integrated into the dual-frequency IF combined observable. Although ten combinations can be generated, four sets of IF combinations can meet the requirement to make full of the five-frequency observations. The E1/E5a, E1/E5b, E1/E5 and E1/E6 dual-frequency IF combinations are utilized, whose noise amplification factors are smaller than other combination. The FF1 model with m satellites can be written as:

$$\left\{ \begin{bmatrix} P_{FF1} \\ \Phi_{FF1} \end{bmatrix} = \left[e_8 \otimes B, e_8 \otimes e_m, n_2' \otimes (d_4 \otimes I_m), n_2 \otimes (C^T \cdot \Lambda \otimes I_m) \right] \begin{bmatrix} x \\ \bar{t}_r \\ ifb_{FF1} \\ a \end{bmatrix} + \begin{bmatrix} \varepsilon_{P,FF1} \\ \varepsilon_{\Phi,FF1} \end{bmatrix}, \right.$$

$$\begin{bmatrix} C^T \cdot (q \otimes c_P) \cdot C & \\ & C^T \cdot (q \otimes c_\Phi) \cdot C \end{bmatrix} \otimes Q_m$$

(3)

a denotes the vector of the ambiguities.

2.4. FF2: Model with a five-frequency IF combined observable

The five-frequency Galileo measurements can be grouped into a designated combination with the criteria that are geometry-free, IF and have minimum noise. The criteria to determine the coefficients $k^T = [k_1, k_2, k_3, k_4, k_5]$ can be given as:

$$\begin{cases} e^T \cdot k = 1 \\ u^T \cdot k = 0 \\ F = k^T \cdot q \cdot k = min \end{cases}$$

(4)

where $u^T = [1, u_2, u_3, u_4, u_5], u_k = (f_1/f_k)^2, (k = 2, 3, 4, 5)$.

The coefficients following the above criteria can be solely determined as follows (the derivation of the coefficients is given in Appendix):

$$k = \begin{bmatrix} \dfrac{(u_2 - u_2^2) \cdot q_3^2 \cdot q_4^2 \cdot q_5^2 + (u_3 - u_3^2) \cdot q_2^2 \cdot q_4^2 \cdot q_5^2 + (u_4 - u_4^2) \cdot q_2^2 \cdot q_3^2 \cdot q_5^2 + (u_5 - u_5^2) \cdot q_2^2 \cdot q_3^2 \cdot q_4^2}{E} \\[2mm] \dfrac{(u_2 - 1) \cdot q_3^2 \cdot q_4^2 \cdot q_5^2 + (u_2 \cdot u_3 - u_3^2) \cdot q_1^2 \cdot q_4^2 \cdot q_5^2 + (u_2 \cdot u_4 - u_4^2) \cdot q_1^2 \cdot q_3^2 \cdot q_5^2 + (u_2 \cdot u_5 - u_5^2) \cdot q_1^2 \cdot q_3^2 \cdot q_4^2}{E} \\[2mm] \dfrac{(u_3 - 1) \cdot q_2^2 \cdot q_4^2 \cdot q_5^2 + (u_2 \cdot u_3 - u_2^2) \cdot q_1^2 \cdot q_4^2 \cdot q_5^2 + (u_3 \cdot u_4 - u_4^2) \cdot q_1^2 \cdot q_2^2 \cdot q_5^2 + (u_3 \cdot u_5 - u_5^2) \cdot q_1^2 \cdot q_2^2 \cdot q_4^2}{E} \\[2mm] \dfrac{(u_4 - 1) \cdot q_2^2 \cdot q_3^2 \cdot q_5^2 + (u_2 \cdot u_4 - u_2^2) \cdot q_1^2 \cdot q_3^2 \cdot q_5^2 + (u_3 \cdot u_4 - u_3^2) \cdot q_1^2 \cdot q_2^2 \cdot q_5^2 + (u_4 \cdot u_5 - u_5^2) \cdot q_1^2 \cdot q_2^2 \cdot q_3^2}{E} \\[2mm] \dfrac{(u_5 - 1) \cdot q_2^2 \cdot q_3^2 \cdot q_4^2 + (u_2 \cdot u_5 - u_2^2) \cdot q_1^2 \cdot q_3^2 \cdot q_4^2 + (u_3 \cdot u_5 - u_3^2) \cdot q_1^2 \cdot q_2^2 \cdot q_4^2 + (u_4 \cdot u_5 - u_4^2) \cdot q_1^2 \cdot q_2^2 \cdot q_3^2}{E} \end{bmatrix}$$

(5)

where $n_2' = [1, 0]^T$; $d_4 = \text{diag}(0, 1, 1, 1)$; $C^T =$

$$\begin{bmatrix} \alpha_{(1,2)} & \beta_{(1,2)} & 0 & 0 & 0 \\ \alpha_{(1,3)} & 0 & \beta_{(1,3)} & 0 & 0 \\ \alpha_{(1,4)} & 0 & 0 & \beta_{(1,4)} & 0 \\ \alpha_{(1,5)} & 0 & 0 & 0 & \beta_{(1,5)} \end{bmatrix};$$

$\Lambda = \text{diag}(\lambda_1, \lambda_2, \lambda_3, \lambda_4, \lambda_5)$; $a^T =$ $[a_1^T, a_2^T, a_3^T, a_4^T, a_5^T]$ denotes the vector of the ambiguities; $q = \text{diag}(q_1^2, q_2^2, q_3^2, q_4^2, q_5^2)$; ifb_{FF1} denotes the estimated IFB vector in FF1 model. Owing to the four IF combined observables share the same estimated receiver clock values, three estimable IFB parameters with regard to the E1/E5b, E1/E5 and E1/E6 pseudorange combinations are mandatory to account for the inconsistency of pseudorange observables and the receiver clock.

with

$$E = -q_3^2 \cdot q_4^2 \cdot q_5^2 \cdot (u_2 - 1)^2 - q_2^2 \cdot q_4^2 \cdot q_5^2 \cdot (u_3 - 1)^2 - q_2^2 \cdot q_3^2 \cdot q_5^2 \cdot (u_4 - 1)^2$$
$$-q_2^2 \cdot q_3^2 \cdot q_4^2 \cdot (u_5 - 1)^2 - q_1^2 \cdot q_4^2 \cdot q_5^2 \cdot (u_3 - u_2)^2 - q_1^2 \cdot q_3^2 \cdot q_5^2 \cdot (u_4 - u_2)^2$$
$$-q_1^2 \cdot q_3^2 \cdot q_4^2 \cdot (u_5 - u_2)^2 - q_1^2 \cdot q_2^2 \cdot q_5^2 \cdot (u_4 - u_3)^2 - q_1^2 \cdot q_2^2 \cdot q_4^2 \cdot (u_5 - u_3)^2$$
$$-q_1^2 \cdot q_2^2 \cdot q_3^2 \cdot (u_5 - u_4)^2$$

(6)

In view of five-frequency pseudorange observations are grouped into the one observation, the receiver clock will eventually absorb the receiver uncalibrated code delays (UCDs). Hence, the FF2 model with m satellites can be written as:

$$\begin{cases} \begin{bmatrix} \boldsymbol{P}_{FF2} \\ \boldsymbol{\Phi}_{FF2} \end{bmatrix} = \begin{bmatrix} \boldsymbol{e}_2 \otimes \boldsymbol{B}, \boldsymbol{e}_2 \otimes \boldsymbol{e}_m, \boldsymbol{n}_2 \otimes (\boldsymbol{k}^T \cdot \Lambda \otimes \boldsymbol{I}_m) \end{bmatrix} \begin{bmatrix} \boldsymbol{x} \\ \bar{t}_r \\ \boldsymbol{a} \end{bmatrix} + \begin{bmatrix} \boldsymbol{\varepsilon}_{P,FF2} \\ \boldsymbol{\varepsilon}_{\Phi,FF2} \end{bmatrix}, \\ \begin{bmatrix} \boldsymbol{k}^T \cdot (\boldsymbol{q} \otimes c_P) \cdot \boldsymbol{k} & \\ & \boldsymbol{k}^T \cdot (\boldsymbol{q} \otimes c_\Phi) \cdot \boldsymbol{k} \end{bmatrix} \otimes \boldsymbol{Q}_m \end{cases} \quad (7)$$

2.5. Model using five-frequency UC observables

Distinguishing from IF based models, the slant ionospheric delays are estimated as unknowns in FF3 model. The FF3 model with m satellites can be written as:

$$\begin{cases} \begin{bmatrix} \boldsymbol{P}_{FF3} \\ \boldsymbol{\Phi}_{FF3} \end{bmatrix} = \begin{bmatrix} \boldsymbol{e}_{10} \otimes \boldsymbol{B}, \boldsymbol{e}_{10} \otimes \boldsymbol{e}_m, \boldsymbol{n}'_2 \otimes (\boldsymbol{d}_5 \otimes \boldsymbol{I}_m), \boldsymbol{n}''_2 \otimes (\boldsymbol{u} \otimes \boldsymbol{I}_m), \boldsymbol{n}_2 \otimes (\Lambda \otimes \boldsymbol{I}_m) \end{bmatrix} \begin{bmatrix} \boldsymbol{x} \\ \bar{t}_r \\ \boldsymbol{ifb}_{FF3} \\ \boldsymbol{\tau} \\ \boldsymbol{a} \end{bmatrix} + \begin{bmatrix} \boldsymbol{\varepsilon}_{P,FF3} \\ \boldsymbol{\varepsilon}_{\Phi,FF3} \end{bmatrix}, \\ \begin{bmatrix} \boldsymbol{q} \otimes c_P & \\ & \boldsymbol{q} \otimes c_\Phi \end{bmatrix} \otimes \boldsymbol{Q}_m \end{cases} \quad (8)$$

where $\boldsymbol{d}_5 = \mathrm{diag}(0,0,1,1,1); \boldsymbol{n}''_2 = [1,-1]^T$. In FF3 model, the linearly related slant ionospheric delay and receiver E1/E5a DCB parameters are estimated as lumped terms and cannot be separated. $\boldsymbol{ifb}_{FF3}$ denotes the estimated IFB vector in FF3 model. Parallel to the FF1 model, the IFB parameters are also required to compensate the inconsistency of receiver UCDs on E5b, E5 and E6 frequencies.

2.6. Model using five-frequency UC observables with external ionospheric constraint

In FF4 model, the external ionospheric constraints are added on the estimated ionospheric delays by the ionospheric virtual observations. Meanwhile, the receiver DCB and pure slant ionosphere delay can be estimated separately. Hence, the FF4 model with m satellites can be written as:

$$\begin{cases} \begin{bmatrix} \boldsymbol{P}_{FF4} \\ \boldsymbol{\Phi}_{FF4} \end{bmatrix} = \begin{bmatrix} \boldsymbol{e}_{10} \otimes \boldsymbol{B}, \boldsymbol{e}_{10} \otimes \boldsymbol{e}_m, \boldsymbol{n}'_2 \otimes (\boldsymbol{d}_5 \otimes \boldsymbol{I}_m), \boldsymbol{n}'_2 \otimes (\boldsymbol{n}'_5 \otimes \boldsymbol{I}_m), \boldsymbol{n}''_2 \otimes (\boldsymbol{u} \otimes \boldsymbol{I}_m), \boldsymbol{n}_2 \otimes (\Lambda \otimes \boldsymbol{I}_m) \end{bmatrix} \begin{bmatrix} \boldsymbol{x} \\ \bar{t}_r \\ \boldsymbol{ifb}_{FF4} \\ DCB \\ \boldsymbol{\tau} \\ \boldsymbol{a} \end{bmatrix} + \begin{bmatrix} \boldsymbol{\varepsilon}_{P,FF4} \\ \boldsymbol{\varepsilon}_{\Phi,FF4} \end{bmatrix}, \\ \begin{bmatrix} \boldsymbol{q} \otimes c_P & \\ & \boldsymbol{q} \otimes c_\Phi \end{bmatrix} \otimes \boldsymbol{Q}_m, \\ \boldsymbol{\tau}_0 = \boldsymbol{\tau}, \sigma_\tau^2 \end{cases} \quad (9)$$

where $\boldsymbol{n}'_5 = \begin{bmatrix} \beta_{(1,2)}, -\alpha_{(1,2)}, u_3 \cdot \beta_{(1,2)}, u_4 \cdot \beta_{(1,2)}, u_5 \cdot \beta_{(1,2)} \end{bmatrix}^T$; DCB denotes the estimated receiver DCB parameter; $\boldsymbol{\tau}_0$ is the external ionospheric observable, which can be provided by the external products such as global ionosphere map (GIM).

2.7. Discussion on the five-frequency PPP models

Table 1 compares the dual-, triple- and five-frequency Galileo PPP models in terms of the adopted observations, coefficients, ionospheric delay factor with respect to the Galileo E1 part and the noise amplification factors. Furthermore, Table 2 provides the characteristics of the estimated parameters of the dual-, triple- and five-frequency PPP models when observing the m satellites. In fact, the introduced five-frequency PPP models can be considered as the different forms of the same Galileo input data including the pseudorange and carrier phase observations. More specifically, the observables in the FF1 and FF2 models are passed through a linear transformation process to the raw observations where the corresponding coefficient matrix is invertible. Similarly, the variance–covariance matrix and the solution vector are identical with the transformed equations based on the algebraic theory [33]. That is to say, owing to the weight matrices are determined following the law of covariance propagation, the FF1, FF2 and FF3 models are theoretically equivalent as along as the estimated ionospheric delay and receiver hardware delay are estimated as white noises [34]. For a different situation, the external information added on the FF4 model will lead to a different PPP performance.

For simplicity, we consider that the Galileo five-frequency observations share the same prior noise though the different frequencies may have different characteristics [28]. The prior noise δ_0^2 can be expressed as a Sine mapping function i.e. $\delta_0 = a/sin(E)$, in which a denotes the observation precision. Compared with raw observables, the noise amplification factors of IF-based combinations range from 2.4 to 3.5 depending on the frequency combination. The E1/E5a combined observable in FF1 model provides the best priori performance among the four IF combinations and the nonzero off-diagonal elements of covariance matrix indicate that the different IF combinations have the strong correlations. The five-frequency IF combined observable in FF2 model shows the smaller combination noise than any other IF combinations. The FF1, FF2 and FF3 models employed with the Kalman filter have internal equivalence when the filter has fully converged, where at that

Table 1
Comparison of dual-, triple and five-frequency PPP models.

Models	Obs	E_1	E_2	E_3	E_4	E_5	Ion	Noise
DF	E1/E5a	2.261	−1.261	0	0	0	0	2.588
TF	E1/E5a/E5b	2.315	−0.836	−0.479	0	0	0	2.507
FF1	E1/E5a	2.261	−1.261	0	0	0	0	2.588
	E1/E5b	2.422	0	−1.422	0	0	0	2.809
	E1/E5	2.338	0	0	−1.338	0	0	2.694
	E1/E6	2.931	0	0	0	−1.931	0	3.510
FF2	Aʟʟ	2.217	−0.680	−0.351	−0.512	0.326	0	2.423
FF3/FF4	E1	1	0	0	0	0	1	1
	E5a	0	1	0	0	0	1.793	1
	E5b	0	0	1	0	0	1.703	1
	E5	0	0	0	1	0	1.747	1
	E6	0	0	0	0	1	1.518	1

Table 2
Characteristics of the parameters for the dual-, triple and five-frequency PPP models.

Models	Raw observed number	Estimated parameter number	Redundancy
DF	2m	m+5	m − 5
TF	2m	m+5	m − 5
FF1	8m	4 m+8	4m − 8
FF2	2m	m+5	m − 5
FF3	10m	6 m+8	4m − 8
FF4	11m	6 m+9	5m − 9

time the ionospheric delay and phase ambiguity parameters are effectively and successfully separated.

3. Performance and evaluation

In this section, we begin with the introduction of the Galileo-only PPP data processing strategies. Then, datasets provided by the MGEX network are used to verify the static PPP performance in terms of convergence time and positioning accuracy. Furthermore, the receiver clock, tropospheric delay, receiver IFBs, and DCB estimates are analyzed. Finally, the kinematic PPP performance are analyzed.

3.1. Data processing strategies

To validate the Galileo-only five-frequency PPP performance, datasets of 26 MGEX stations capable of observing the Galileo five-frequency observations are collected from day of year (DOY) 1-30, 2019, for static PPP test. A dynamic experiment on the campus playground was conducted to perform the kinematic PPP tests. Fig. 1 shows the geographical distribution of the selected 26 MGEX stations. Table 3 summarizes the receivers and antenna type of the contributing MGEX stations. The selected stations all can observe the five-frequency measurements though the different receivers may not have exactly the same settings including the bandwidth, filtering strategy, multipath mitigation, the strategy of obtaining the special measurement and so on. Table 4

Fig. 1. Geographical distribution of the selected 26 MGEX stations.

Table 3
Receivers and antenna type of the contributing 26 MGEX stations.

Station	Receiver type	Antenna type
AREG, HARB, PTGG, TLSG, TONG	SEPT POLARX5	TRM59800.00
GAMG, GOP6, STJ3, YEL2		LEIAR25.R4
KAT1, KOUG		LEIAR25.R3
DARW, LAUT, POHN		JAVRINGANT_DM
YAR3		LEIAR25
YARR		LEIAT504
NRMG		TRM57971.00
STR1		ASH701945C_M
BRST	TRIMBLE ALLOY	TRM57971.00
KZN2	TRIMBLE NETR9	TRM59800.00
LPGS, POTS, SGOC, ULAB, URUM, WUH2	JAVRINGANT_G5T	JAVAD TRE_3

summarizes the detailed processing strategy of Galileo five-frequency PPP as well as Galileo dual- and triple-frequency PPP models for the selected stations. The Galileo code and phase observation precision are set to 0.4 m and 0.004 m, respectively [24]. The position coordinates are modeled as constants and white noise in static and kinematic PPP modes, respectively. The positioning performance is assessed with

Table 4
Galileo PPP data processing strategy.

| Items	Strategies
Solutions	DF, TF, FF1, FF2, FF3 and FF4
Observations	Galileo E1, E5a, E5b, E5 and E6 pseudorange and carrier phase observations
Sampling rate	Static data: 30 s; kinematic data: 1 s
Elevation cutoff	7°
Satellite orbit	Fixed by GFZ precise orbit products
Satellite clock	Fixed by GFZ precise clock products
Satellite DCB	E1: $-\beta^s_{(1,2)} \cdot DCB^s_{(1,2)}$; E5a: $\alpha^s_{(1,2)} \cdot DCB^s_{(1,2)}$; E5b: $DCB^s_{(1,3)} -\beta^s_{(1,2)} \cdot DCB^s_{(1,2)}$; E5: $DCB^s_{(1,4)} -\beta^s_{(1,2)} \cdot DCB^s_{(1,2)}$; E6: $DCB^s_{(1,5)} -\beta^s_{(1,2)} \cdot DCB^s_{(1,2)}$; Corrected with Chinese Academy of Sciences (CAS) products [38]
Earth rotation	Fixed [18]
Relativistic effect	Corrected [39]
Phase windup effect	Corrected [40]
Tide effect	Solid Earth, pole and ocean tide [18]
Satellite and receiver antenna	MGEX values. When the phase center corrections on the third, fourth and fifth frequency are unavailable, the corrections on the second frequency are applied.
Station coordinates	Static: estimated as constants; Kinematic: estimated as white noise process (100 m²)
Receiver clock	Estimated as white noises (10^5 m²/s)
Tropospheric delay	Dry component: GPT3 model together with Modified Hopfield; Wet component: estimated as random part (10^{-9} m²/s), VMF3 mapping function [41,42]
Receiver DCB and IFB	Absorbed by receiver clock or estimated as constants
Ionospheric delay	DF/TF/FF1/FF2: eliminated by IF observations; FF3/FF4: estimated as white noise process (10^4 m²/s) [22,43]
Ambiguities	Estimated as constant
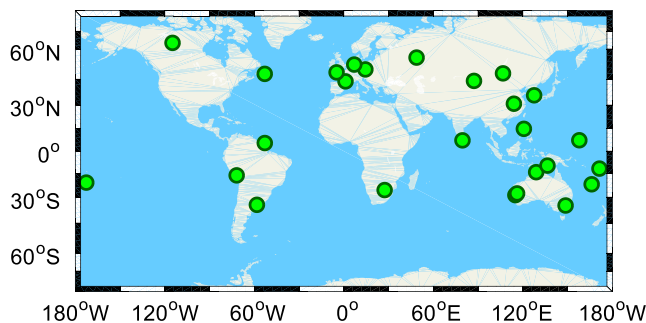
respect to the coordinates from IGS solutions. Owing to the different observations are applied with the same satellite clock estimates, the disagreement defined as inter-frequency clock bias (IFCB) arises. The consistency of Galileo five-frequency time-dependent UCDs can be ensured and thus the IFCB in Galileo can be neglected [35]. The GIM

provided by IGS, with an accuracy of few total electronic content units (TECUs) is used for the prior ionosphere constraint. The variance of the virtual ionospheric parameters for GIM can refer to the literature [22]. The FF4 model can also be carried out with some other high-accuracy ionospheric models that used as the constraints [36,37].

3.2. Static PPP performance

The static PPP performance is investigated and assessed in terms of convergence time and positioning accuracy. The convergence criterion is defined as the three-dimensional positioning errors are less than the 10 cm at the current epoch and keep the feature during the following twenty epochs [44]. The three-dimensional root mean square (RMS) is calculated using the positioning errors from the convergent epoch to the end epoch in a day. Taking the stations DARW and GAMG on DOY 001/ 2019 as the examples, Fig. 2 shows the positioning error of Galileo-only static PPP for DF, TF, FF1, FF2, FF3 and FF4 models, respectively. We can observe that the positioning errors are within 2 cm in the north, east and up components for the dual-, triple- and five-frequency PPP models at two stations. The positioning solutions of the FF1, FF2 and FF3 models exhibit the great agreement, and show slightly better performance than the DF and TF solutions. The difference between FF4 and other PPP models mainly lies in the initial time, which is influenced by the constraints from the external ionospheric products.

Fig. 3 illustrates the distribution and boxplot of the Galileo-only static PPP convergence time with different models for 26 MGEX stations. Moreover, Fig. 4 provides the three-dimensional RMS of Galileo-only static PPP by different models. For each boxplot, it has five horizontal lines, representing 0%, 25%, 50%, 75% and 100% quantiles from bottom to top, respectively. The median and mean of corresponding values are also provided in the figures. It is apparent that the positioning performance of FF1, FF2 and FF3 agrees well with each other, for instance, of which the median values (50% quantiles) of convergence time are 30.5, 30.5, 31.0 min, respectively. It is no surprising for that their equivalence has been discussed. A slightly difference can be found between FF3 model and IF based PPP models in that the correlation exists between the estimable ionospheric delay parameters and phase ambiguity parameters in FF3 model before convergence. The convergence performance of Galileo-only FF4 solution exhibits much worse than other PPP models, which is influenced by the limited accuracy of GIM (2–8 TECU) [45]. The similar phenomena existed in dual-frequency PPP has been demonstrated by Zhou et al [46]. In addition, compared with Galileo-only dual-frequency IF model, the positioning accuracy of five-frequency PPP models is effectively improved after convergence. The growing weighting of ionospheric virtual observations have subtle influence on the positioning accuracy of Galileo-only FF4 scheme in the filter process after convergence.
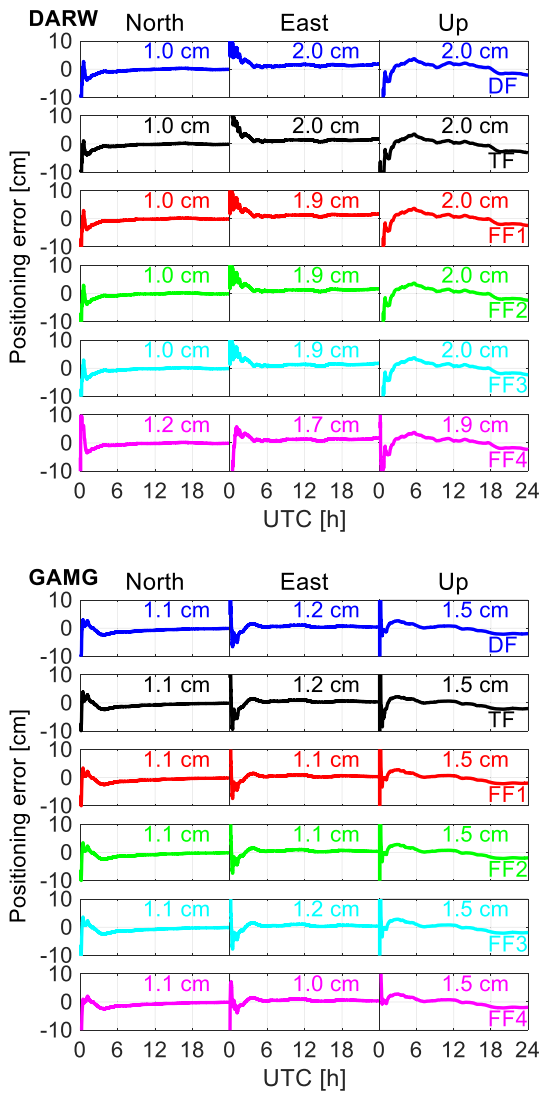

Fig. 2. Positioning error of Galileo-only static PPP solutions among different PPP models at stations DARW (top) and GAMG (bottom) (DOY 001/2019).
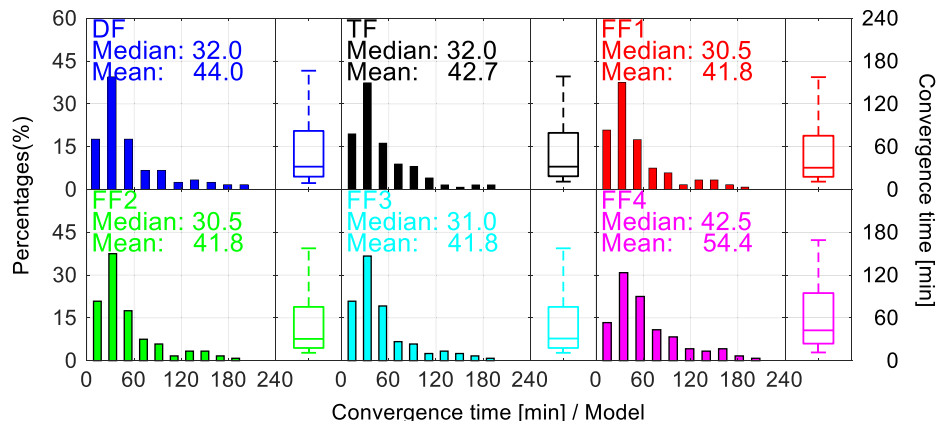

Fig. 3. Distribution and boxplot of the Galileo-only static PPP convergence time with DF, TF, FF1, FF2, FF3 and FF4 schemes for the selected 26 stations.
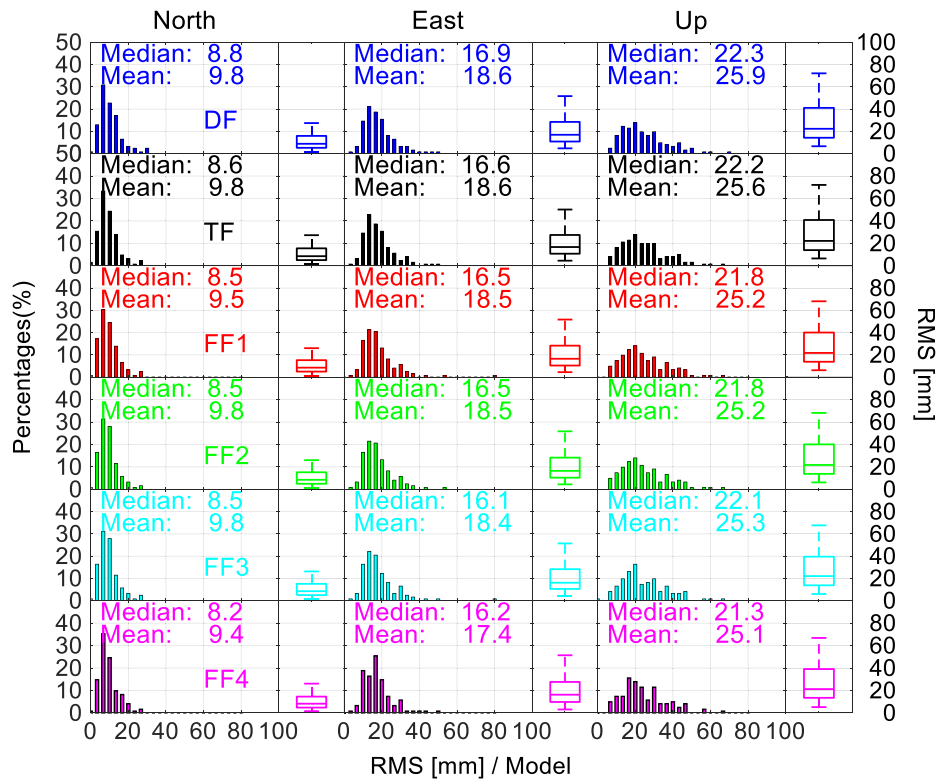
Fig. 4. Distribution and boxplot of the three-dimensional RMS of Galileo-only static PPP with DF, TF, FF1, FF2, FF3 and FF4 schemes for the selected 26 stations.
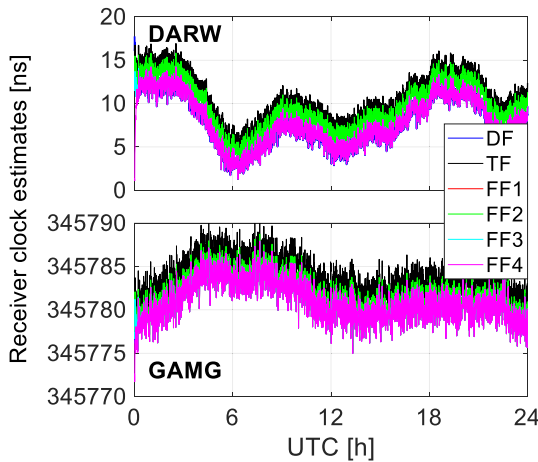

Fig. 5. Time series of the estimated receiver clock time series for different Galileo-only PPP models at stations DARW and GAMG.

Fig. 6. Estimated ZTD time series of stations DARW and GAMG for different Galileo-only PPP models at stations DARW and GAMG.

3.3. Receiver clock, tropospheric delay, receiver IFB and DCB estimates

Fig. 5 depicts the estimated receiver clock time series for different Galileo-only PPP models at stations DARW and GAMG. Slight differences exist for the receiver clock estimates of DF, TF and five-frequency PPP models, especially for the station DRAW. The estimated receiver clock of two stations fluctuates less than 15 ns in one day. The clock time series of stations DARW and GAMG show the different variation tendency due to the common unmodelled error. The receiver clocks in DF, FF1, FF3 and FF4 models refer to the same values, that are the combined raw receiver clock and Galileo E1/E5a receiver UCDs ($d\bar{t}_r = dt_r + d_{r,(1,2)}$). The values in FF2 model with a systematic bias show the same variation ($d\bar{t}_r = dt_r + d_{r,(1,2,3,4,5)}$).

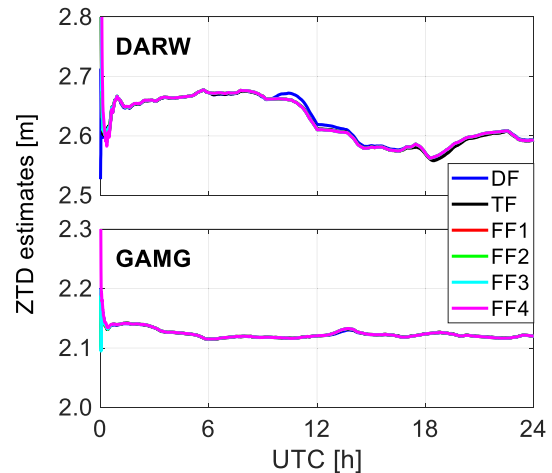Fig. 6 shows the estimated ZTD series for different PPP models at two

stations, which are estimated as random-walk process in the models. The estimable ZTDs can be segmented into the estimated ZWDs and priori zenith hydrostatic delays (ZHDs) derived by the GPT3 and Modified Hopfield models. To evaluate the accuracy estimated ZTDs, the values provided by IGS with a typical formal accuracy of 1.5–5 mm are used as the reference [47]. The RMS of the ZTD errors are (1.6, 1.5, 1.5, 1.5, 1.5, 1.5) cm and (0.9, 0.9, 0.9, 0.9, 0.9, 0.9) cm for stations DARW and GAMG, respectively, for the DF, TF, FF1, FF2, FF3 and FF4 models. Like the estimated receiver clocks, the ZTDs differences mainly exist among the DF and PPP models, especially for the station DRAW as well. The differences of estimated ZTDs from the five-frequency PPP models are small and can be neglectable after convergence.

The receiver IFB values have to be estimated in FF1, FF3 and FF4 models. Fig. 7 shows the time series of IFB estimates at stations DRAW
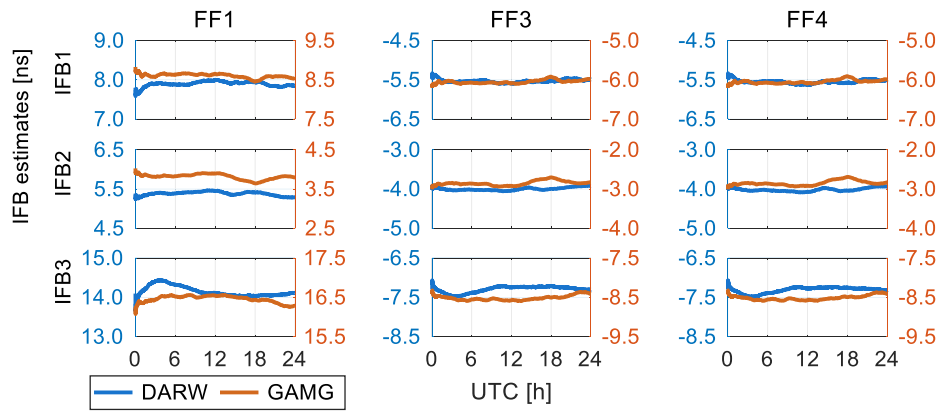
Fig. 7. Receiver IFB estimates of the five-frequency Galileo-only FF1, FF3 and FF4 models on stations DRAW and GAMG (DOY 001/2019).
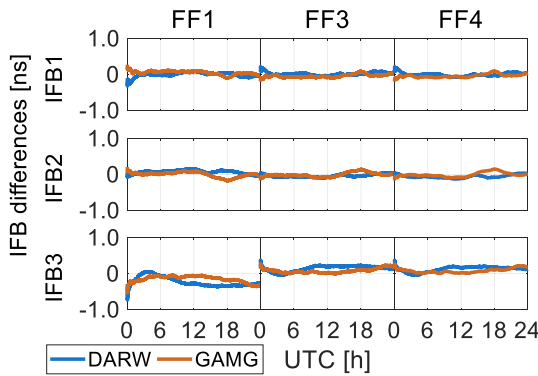

Fig. 8. Difference of receiver IFB estimates with respect to MGEX reference IFBs on stations DRAW and GAMG (DOY 001/2019).
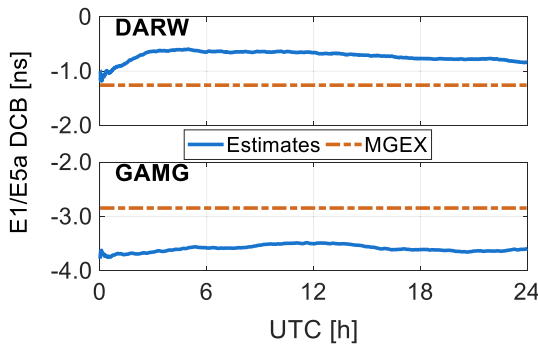

Fig. 9. Receiver E1/E5a DCB estimates together with MGEX reference DCBs on stations DRAW and GAMG (DOY 001/2019).

and GAMG, respectively. The IFB estimates are epoch-wise and stable. Hence, it is possible to estimate the IFBs as constants in a day. The maximum variations of receiver IFBs in three models are less than 0.5 ns (equivalent to 0.15 m). In fact, the ratio of estimated IFB1, IFB2 and IFB3 in the FF1 and FF3 (FF4) models theoretically are $\beta_{(1,3)}^s$ (-1.422), $\beta_{(1,4)}^s$ (-1.388) and $\beta_{(1,5)}^s$ (-1.931), respectively. To further verify the estimated IFBs accuracy for the three models, Galileo receiver DCBs (i,e., $DCB_{r,(1,3)}$, $DCB_{r,(1,4)}$ and $DCB_{r,(1,5)}$) extracted from the MGEX products are used to calculate the reference IFB values. Fig. 8 shows the receiver IFB estimates difference with respect to MGEX reference IFBs at two stations. The results indicate that the differences are all within 0.3 ns (equivalent to 0.09 m). We can conclude that the estimated IFBs have an accuracy of few centimeters.

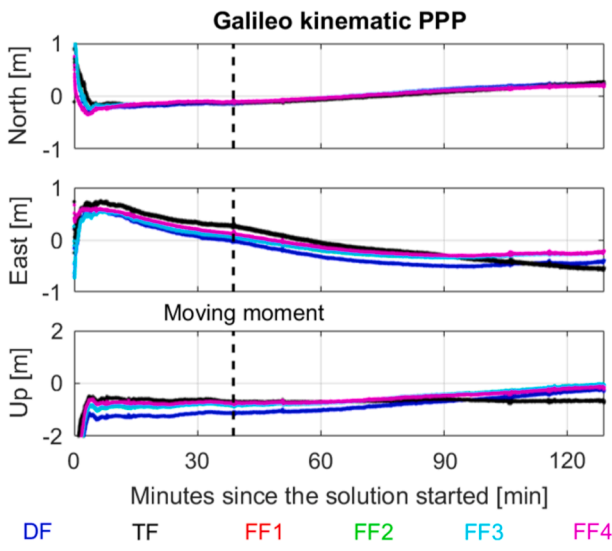**Fig. 10.** Trajectory of the rover station and the location of the reference station.

Furthermore, there is an additional estimated receiver DCB parameter in FF4 model. Fig. 9 shows the receiver E1/E5a DCB estimates at two stations. The MGEX reference DCB values are depicted for comparison. The RMS of estimated DCBs are 0.55 and 0.75 ns, respectively, with regard to the reference values. The relatively lower accuracy of estimated DCBs arises from the limited accuracy of GIM products and the strong correlation between DCB and the slant ionospheric delay.

3.4. Kinematic PPP tests

To validate the Galileo-only five-frequency PPP performance in real kinematic scenarios, a dynamic experiment was conduct on the Zhongyuan old playground of the campus of Nanjing University of Information Science and Technology in Nanjing, China on December 26, 2019. The experiment begins at the GPS time 06:37:02 and lasts for more than two hours. The kinematic data have the sampling rate of 1 Hz with the cut-off angle of 7°. Fig. 10 shows the trajectory of the rover station as well as the location of the reference station. For the reference station, the TRIMBLE ALLOY receiver was equipped with TRM57971.00 antenna. The rover station with the same receiver and antenna types was taken by the experimenters to walk around the playground for five times after resting for approximately 30 min. The multi-GNSS ambiguity-fixed double-difference real-time kinematic (RTK) approach was handled to provide the reference values for the Galileo-only kinematic PPP tests [14]. From Fig. 10, we can observe that distances between the rover and reference stations are always less than 400 m during the experimental period.

The Galileo-only kinematic PPP kinematic positioning errors of the DF, TF, FF1, FF2, FF3 and FF4 solutions with reference to the RTK

Galileo kinematic PPP

DF   TF   FF1   FF2   FF3   FF4

(a) Galileo kinematic PPP

Galileo and GPS/Galileo kinematic PPP

DF (E)   DF (G+E)
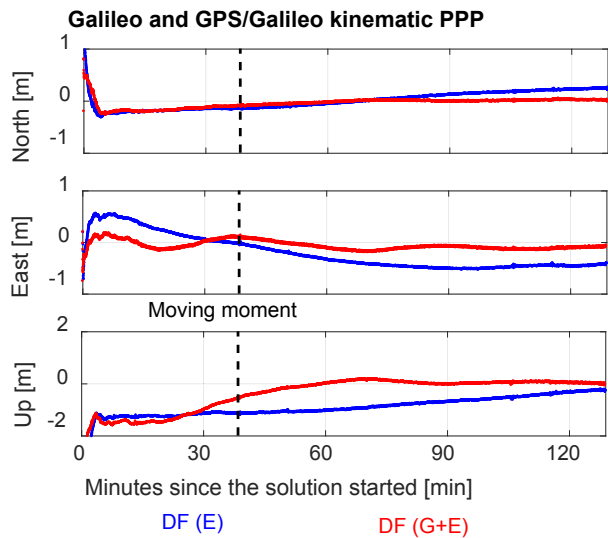
(b) Galileo and GPS/Galileo kinematic PPP

Fig. 11. Positioning errors for the Galileo-only and GPS/Galileo kinematic PPP solutions.
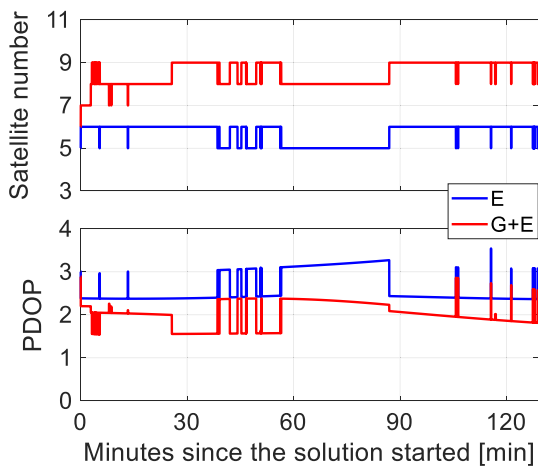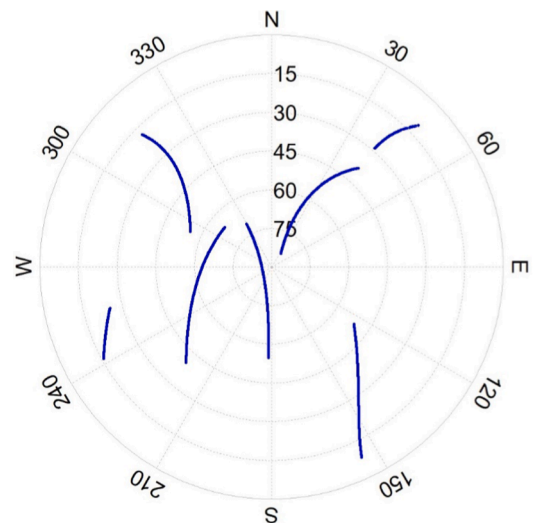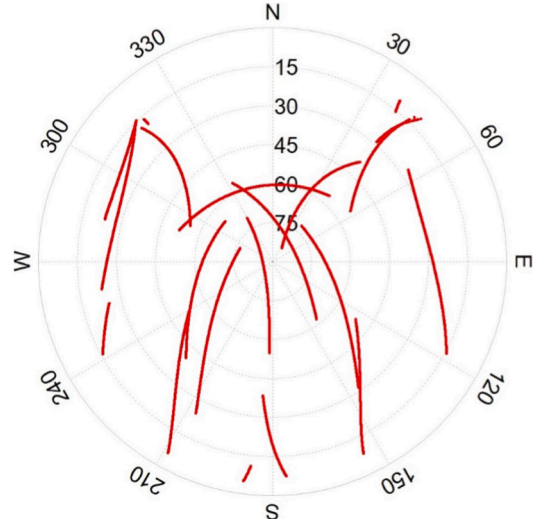

Fig. 12. Visible Galileo and GPS/Galileo satellite number and corresponding PDOP values.

(a) Galileo

(b) GPS + Galileo

Fig. 13. Sky plots of Galileo and GPS/Galileo satellites at the rover station.

Table 5
Accuracy of the Galileo kinematic PPP models.

Accuracy	North (cm)	East (cm)	Up (cm)	3-D (cm)
DF	14.7	43.4	72.6	85.9
TF	13.1	34.1	66.1	75.5
FF1	12.5	27.5	49.7	58.2
FF2	12.5	27.6	49.6	58.1
FF3	12.6	27.7	49.6	58.2
FF4	12.1	24.8	50.4	57.4
DF (G+R)	2.1	11.3	8.2	14.1

solution in the north, east and up components, respectively, are shown in Fig. 11. The positioning performance of the Galileo-only PPP seems to perform not very well, which is expected given the lower number of Galileo satellites. To demonstrate it, Fig. 11 also provides the Galileo-only and GPS/Galileo kinematic PPP kinematic positioning errors in three components. Furthermore, Fig. 12 depicts the visible satellite number and corresponding positioning dilution of precision (PDOP) values of the Galileo and GPS/Galileo system. The mean values for the visible Galileo and GPS/Galileo satellite number are 5.7 and 8.5, respectively, and the corresponding PDOP values are 2.6 and 2.0. Fig. 13 shows the sky plot of the Galileo and GPS/Galileo satellites for the rover

station. During the whole experiment period, only Galileo satellites E02, E03, E05, E08, E24 and E30 can be observed. The observed Galileo satellite number is relatively limited in the tested region.

To evaluate the Galileo kinematic PPP positioning accuracy, Table 5 shows the root mean square (RMS) values of the positioning errors for different kinematic PPP solutions since the rover station moved, in which the initialization phase is end and the three-dimension positioning errors have been relative stable. The positioning accuracy of FF1, FF2 and FF3 is as well basically the same in kinematic scenarios. However, distinguished from the static PPP solutions, the positioning accuracy of Galileo five-frequency PPP is significantly improved compared with the dual- and triple-frequency solutions. For instance, compared with Galileo-only DF scheme, the positioning accuracy of the FF3 solution can be improved by 14.3%, 36.2% and 31.7% in the north, east and up components, respectively. The contribution of the multi-frequency signals in PPP is obvious and can improve the positioning accuracy and reliability in real kinematic situations. The performance of the Galileo-only kinematic PPP is relatively poor and mainly affected by the limited observed satellites. Only 5–6 Galileo satellites can be observed during the whole experimental period. By adding the GPS observations, it's apparent that the positioning accuracy of the DF solution is improved by 85.7%, 74.0% and 83.6% in three directions. With the inclusion of the ionosphere constraint, the Galileo five-frequency PPP 3-D positioning accuracy is slightly improved at approximately 0.8 cm, which is influenced by that the estimated ionospheric delay parameters and receiver DCB are effectively separated.

4. Conclusion

In this contribution, we develop the five-frequency Galileo PPP models and evaluate the corresponding performance. The Galileo-only dual- and triple-frequency IF PPP solutions are also conducted for comparison. The former two models use IF combinations, and latter two models employ the raw measurements. With the additional observations, receiver IFBs need to be considered in FF1, FF3 and FF4 models.

The receiver E1/E5a DCB also needs to be considered in FF4 model.

Statistical results indicate that the positioning errors have an accuracy of few millimeters in three-dimensional components for dual-, triple and five-frequency PPP models in static scenarios. The kinematic PPP solutions have an accuracy of decimeter level. The positioning accuracy of the north component is the best, followed by the east and up components. By comparing the results among FF1, FF2, and FF3 schemes, their performance has shown great consistencies. The convergence time of FF4 model is deteriorated for the static datasets, but the positioning accuracy is improved, especially obvious for the kinematic scenarios. Compared to dual- and triple-frequency IF PPP, the positioning performance of Galileo five-frequency PPP in terms of positioning accuracy and convergence time is both improved.

CRediT authorship contribution statement

Ke Su: Methodology, Software, Data curation, Writing - original draft. **Shuanggen Jin:** Validation, Writing - review & editing.

Declaration of Competing Interest

The authors declare that they have no known competing financial interests or personal relationships that could have appeared to influence the work reported in this paper.

Appendix A

In this part, we give the coefficients derivation in FF2 model. Rearranging Eq. (4) gives:

$$F = \boldsymbol{k}^T \cdot \boldsymbol{q} \cdot \boldsymbol{k} + \xi_1 \cdot (\boldsymbol{e}^T \cdot \boldsymbol{k} - 1) + \xi_2 \cdot \boldsymbol{u}^T \cdot \boldsymbol{k} \tag{A1}$$

where ξ_1 and ξ_2 are also unknown parameters.

The partial derivatives of the function regarding to $\boldsymbol{k}$ can be expressed as:

$$\begin{cases} \partial F/\partial k_1 = 2 \cdot q_1^2 \cdot k_1 + \xi_1 + \xi_2 = 0 \\ \partial F/\partial k_2 = 2 \cdot q_2^2 \cdot k_2 + \xi_1 + \xi_2 \cdot u_2 = 0 \\ \partial F/\partial k_3 = 2 \cdot q_3^2 \cdot k_3 + \xi_1 + \xi_2 \cdot u_3 = 0 \\ \partial F/\partial k_4 = 2 \cdot q_4^2 \cdot k_4 + \xi_1 + \xi_2 \cdot u_4 = 0 \\ \partial F/\partial k_5 = 2 \cdot q_5^2 \cdot k_5 + \xi_1 + \xi_2 \cdot u_5 = 0 \end{cases} \tag{A2}$$

Then, the above equations can be transformed into:

$$\begin{cases} \xi_1 \cdot A + \xi_2 \cdot B = 0 \\ \xi_1 \cdot C + \xi_2 \cdot A = -2 \cdot D \end{cases} \tag{A3}$$

with

$$\begin{cases}
A = D/q_1^2 + u_2 \cdot D/q_2^2 + u_3 \cdot D/q_3^2 + u_4 \cdot D/q_4^2 + u_5 \cdot D/q_5^2 \\
B = D/q_1^2 + u_2^2 \cdot D/q_2^2 + u_3^2 \cdot D/q_3^2 + u_4^2 \cdot D/q_4^2 + u_5^2 \cdot D/q_5^2 \\
\quad C = D/q_1^2 + D/q_2^2 + D/q_3^2 + D/q_4^2 + D/q_5^2 \\
\quad\quad D = q_1^2 \cdot q_2^2 \cdot q_3^2 \cdot q_4^2 \cdot q_5^2
\end{cases} \tag{A4}$$

Squaring Eq. A(3) gives

$$\begin{cases}
\xi_1 = \dfrac{2 \cdot B \cdot D}{A^2 - B \cdot C} \\[2mm]
\xi_2 = \dfrac{-2 \cdot A \cdot D}{A^2 - B \cdot C}
\end{cases} \tag{A5}$$

Substituting Eq. A(4) and Eq. A(5) into Eq. A(2), the coefficients can be obtained successfully.

References

[1] G. ICD, Navstar GPS Space Segment/Navigation User Interfaces, Interface Specification, 2012.
[2] S. Jin, K. Su, PPP models and performances from single-to quad-frequency BDS observations, Satellite Navigation 1 (1) (2020) 1–13.
[3] Y. Yang, Y. Xu, J. Li, C. Yang, Progress and performance evaluation of BeiDou global navigation satellite system: data analysis based on BDS-3 demonstration system, Science China Earth Sciences 61 (5) (2018) 614–624.
[4] I. Glonass, Glonass interface control document, Moscow, Russia, Russian Institute of Space Device Engineering, 2008.
[5] J.Á.Á. Rodríguez, M. Irsigler, G.W. Hein, T. Pany, Combined Galileo/GPS frequency and signal performance analysis, in: Proceedings of the 17th International Technical Meeting of the Satellite Division of The Institute of Navigation (ION GNSS 2004), 2004, pp. 632–649.
[6] D. Borio, C. Gioia, Galileo: The added value for integrity in harsh environments, Sensors 16 (1) (2016) 111.
[7] C. Gioia, D. Borio, A. Angrisano, S. Gaglione, J. Fortuny-Guasch, A Galileo IOV assessment: measurement and position domain, GPS Solutions 19 (2) (2015) 187–199.
[8] I. Galileo, Galileo open service, signal in space interface control document (OS SIS ICD), ed: European space agency/European GNSS supervisory authority, 2008.
[9] T.H. Diessongo, T. Schüler, S. Junker, Precise position determination using a Galileo E5 single-frequency receiver, GPS Solutions 18 (1) (2014) 73–83.
[10] X. Li, et al., Triple-frequency PPP ambiguity resolution with multi-constellation GNSS: BDS and Galileo, J. Geod. (2019) 1–18.
[11] R. Tu, P. Zhang, R. Zhang, J. Liu, X. Lu, Modeling and performance analysis of precise time transfer based on BDS triple-frequency un-combined observations, J. Geod. (2018).
[12] J. Geng, J. Guo, H. Chang, X. Li, Toward global instantaneous decimeter-level positioning using tightly coupled multi-constellation and multi-frequency GNSS, J. Geod. 93 (7) (2019) 977–991.
[13] B. Zhang, P. Hou, T. Liu, Y. Yuan, A single-receiver geometry-free approach to stochastic modeling of multi-frequency GNSS observables, J. Geod. 94 (4) (2020) 1–21.
[14] R. Tu, J. Liu, R. Zhang, P. Zhang, X. Huang, X. Lu, RTK model and positioning performance analysis using Galileo four-frequency observations, Adv. Space Res. 63 (2) (2019) 913–926.
[15] K. Wang, A. Khodabandeh, P.J. Teunissen, Five-frequency Galileo long-baseline ambiguity resolution with multipath mitigation, GPS Solutions 22 (3) (2018) 75.
[16] Y. Tian, L. Sui, G. Xiao, D. Zhao, Y. Tian, Analysis of Galileo/BDS/GPS signals and RTK performance, GPS Solutions 23 (2) (2019) 37.
[17] B. Zhang, Y. Chen, Y. Yuan, PPP-RTK based on undifferenced and uncombined observations: theoretical and practical aspects, J. Geod. 93 (7) (2019) 1011–1024.
[18] G. Petit, B. Luzum, IERS conventions (2010)(No. IERS-TN-36), J Bureau International Des Poids et Mesures Sevres, France, 2010.
[19] X. Li, X. Zhang, X. Ren, M. Fritsche, J. Wickert, H. Schuh, Precise positioning with current multi-constellation global navigation satellite systems: GPS, GLONASS, Galileo and BeiDou, Sci. Rep. 5 (2015) 8328.
[20] L. Pan, X. Zhang, J. Liu, A comparison of three widely used GPS triple-frequency precise point positioning models, GPS Solutions 23 (4) (2019) 121.
[21] F. Guo, X. Zhang, J. Wang, X. Ren, Modeling and assessment of triple-frequency BDS precise point positioning, J. Geod. 90 (11) (2016) 1223–1235.
[22] K. Su, S. Jin, Triple-frequency carrier phase precise time and frequency transfer models for BDS-3, GPS Solutions 23 (3) (2019) 86.

[23] A. Afifi, A. El-Rabbany, An improved model for single-frequency gps/galileo precise point positioning, Positioning 6 (02) (2015) 7.
[24] C. Cai, Y. Gao, L. Pan, J. Zhu, Precise point positioning with quad-constellations: GPS, BeiDou, GLONASS and Galileo, Adv. Space Res. 56 (1) (2015) 133–143.
[25] M. Deo, A. El-Mowafy, Triple-frequency GNSS models for PPP with float ambiguity estimation: performance comparison using GPS, Survey Rev. 50 (360) (2018) 249–261.
[26] G. Liu, X. Zhang, P. Li, Improving the performance of galileo uncombined precise point positioning ambiguity resolution using triple-frequency observations, Remote Sens. 11 (3) (2019) 341.
[27] P. Zhang, R. Tu, Y. Gao, R. Zhang, J. Han, Performance of Galileo precise time and frequency transfer models using quad-frequency carrier phase observations, GPS Solut. 24 (2) (2020) 40.
[28] X. Li, et al., Galileo PPP rapid ambiguity resolution with five-frequency observations, GPS Solut. 24 (1) (2020) 24.
[29] V. Duong, K. Harima, S. Choy, D. Laurichesse, C. Rizos, Assessing the performance of multi-frequency GPS, Galileo and BeiDou PPP ambiguity resolution, J. Spat. Sci. 65 (1) (2020) 61–78.
[30] C. Rizos, V. Janssen, C. Roberts, T. Grinter, PPP versus DGNSS, Geomatics World 20 (6) (2012) 18–20.
[31] A. Leick, L. Rapoport, D. Tatarnikov, GPS satellite surveying, John Wiley & Sons, 2015.
[32] K. Su, S. Jin, G. Jiao, Assessment of multi-frequency GNSS PPP models using GPS, Beidou, GLONASS, Galileo and QZSS, Meas. Sci. Technol. 31 (6) (2020), 064008.
[33] B. Schaffrin, E. Grafarend, Generating classes of equivalent linear models by nuisance parameter, Manuscr. Geod 11 (1986) 262–271.
[34] G. Xu, Y. Xu, GPS: theory, algorithms and applications, Springer, 2016.
[35] X. Cao, et al., Uncombined precise point positioning with triple-frequency GNSS signals, Adv. Space Res. 63 (9) (2019) 2745–2756.
[36] X. Wu, X. Hu, G. Wang, H. Zhong, C. Tang, Evaluation of COMPASS ionospheric model in GNSS positioning, Adv. Space Res. 51 (6) (2013) 959–968.
[37] Y. Yuan, N. Wang, Z. Li, X. Huo, The BeiDou global broadcast ionospheric delay correction model (BDGIM) and its preliminary performance evaluation results, Navigation 66 (1) (2019) 55–69.
[38] B. Zhang, P.J. Teunissen, Y. Yuan, H. Zhang, M. Li, Joint estimation of vertical total electron content (VTEC) and satellite differential code biases (SDCBs) using low-cost receivers, J. Geod. 92 (4) (2018) 401–413.
[39] J. Kouba, A guide to using International GNSS Service (IGS) products, ed, 2009.
[40] J.-T. Wu, S.C. Wu, G.A. Hajj, W.I. Bertiger, S.M. Lichten, Effects of antenna orientation on GPS carrier phase, Astrodynamics 1992 (1991) 1647–1660.
[41] D. Landskron, J. Böhm, VMF3/GPT3: refined discrete and empirical troposphere mapping functions, J. Geod. 92 (4) (2018) 349–360.
[42] K. Su, S. Jin, Improvement of multi-GNSS precise point positioning performances with real meteorological data, J. Navigation 71 (6) (2018) 1363–1380.
[43] Y. Yuan, et al., Refining the Klobuchar ionospheric coefficients based on GPS observations, IEEE Trans. Aerosp. Electron. Syst. 44 (4) (2008) 1498–1510.
[44] K. Su, S. Jin, Y. Ge, Rapid displacement determination with a stand-alone multi-GNSS receiver: GPS, Beidou, GLONASS, and Galileo, GPS Solutions 23 (2) (2019) 54.
[45] M. Hernández-Pajares, et al., The IGS VTEC maps: a reliable source of ionospheric information since 1998, J. Geod. 83 (3–4) (2009) 263–275.
[46] F. Zhou, D. Dong, W. Li, X. Jiang, J. Wickert, H. Schuh, GAMP: An open-source software of multi-GNSS precise point positioning using undifferenced and uncombined observations, GPS Solut. 22 (2) (2018) 33.
[47] S.H. Byun, Y.E. Bar-Sever, A new type of troposphere zenith path delay product of the international GNSS service, J. Geod. 83 (3–4) (2009) 1–7.